

Dissociation Dynamics of Nitrous Oxide Molecule in Strong-Field Ionization by Linearly Polarized Laser Pulse

FERAS AFANEH*

*Department of Physics, Faculty of Science, The Hashemite University,
P.O. Box 330127, Zarqa 13133, Jordan*

Received: 09.09.2021 & Accepted: 18.01.2022

Doi: [10.12693/APhysPolA.141.461](https://doi.org/10.12693/APhysPolA.141.461)

*e-mail: afaneh@hu.edu.jo

The dissociative ionization of nitrous oxide molecules induced by 35 fs linearly polarized laser pulses was experimentally investigated. Different dissociation channels are clearly identified from the time-of-flight coincidence spectra. The relative contributions of different double and triple dissociative ionization channels to the total fragment ion yield are deduced from the coincident spectra of these channels. The results show that a significant contribution to the total fragment ion yield arises from the double dissociative ionization channels: the denitrogenation ($\text{N}_2\text{O}^{2+} \rightarrow \text{N}^+ + \text{NO}^+$) and the deoxygenation ($\text{N}_2 + \text{O}^{2+} \rightarrow \text{O}^+ + \text{N}_2^+$). Furthermore, a considerable contribution of the triple dissociative ionization channels to the total fragment ion yield is also observed. The channels $\text{N}^+ + \text{NO}^+$ and $\text{O}^+ + \text{N}_2^+$ can be explained by dissociation via the $X^3\Sigma^-$ and $1^3\Pi$ states of N_2O^{2+} , as the major peaks in the measured kinetic energy release spectra suggested. The angular distributions of the fragment ions N^+ , NO^+ , O^+ , and N_2^+ resulting from the $\text{N}^+ + \text{NO}^+$ and $\text{O}^+ + \text{N}_2^+$ fragmentation channels were also measured. The distributions show a markedly anisotropic behavior. These anisotropic behaviors in the angular distributions can be attributed to the different orientations of the N_2O molecule relative to the laser polarization during the dissociative ionization process.

topics: strong-field ionization, dissociative ionization, molecular fragmentation, nitrous oxide

1. Introduction

Laser-induced molecular ionization and dissociation are of great importance in both fundamental research and applications in quantum physics, molecular physics, chemical physics, and photochemistry [1–6]. For example, a better understanding of laser-induced electronic and nuclear motions that result in the molecular breakup process is a key step toward coherent control of chemical reactions. Because of recent revolutionary developments in coincidence momentum imaging techniques, we can perform so-called “complete” high-resolution measurements of molecular many-particle systems [2, 3]. One of these state-of-the-art coincidence three-dimensional momentum imaging is the so-called cold target recoil ion momentum spectroscopy (COLTRIMS). Using the COLTRIMS technique to study the dissociation dynamics of molecules provides the complete three-dimensional momenta of the fragments and, therefore, their kinetic energy release (KER) and angular distributions. These measurements can, in turn, facilitate an understanding of the dissociation mechanisms.

Nitrous oxide (N_2O) is one of the well-known greenhouse gases and also one of the dominant ozone-depleting substances emitted through human

activities [7]. Therefore, it is interesting to study and understand the molecular dynamics of the dissociative ionization of N_2O . Moreover, because of its linear asymmetrical triatomic structure (where two N atoms are not equivalent in the chemical site), it becomes more important to study the dissociative ionization of N_2O in detail. Dissociative ionization of N_2O^{q+} induced by the interactions with electrons [8–11], photons [12–16], charged ions [17–20], and intense laser fields [21–23] have been extensively studied. In addition, dissociative ionization of N_2O^{q+} has also been studied theoretically [13, 14, 24].

In this work, we report a detailed study on the many-body dissociative ionization of N_2O^{2+} induced by intense femtosecond laser pulses. The momenta of the correlated fragment ions are measured in coincidence, utilizing the COLTRIMS reaction microscope. Through the correlation analysis of the TOF and momentum conservation of ion-pair fragments, two main reaction channels of the laser-induced ion-pair dissociations are identified, and the corresponding KER distributions are derived. The two-body fragmentation mechanisms of N_2O^{2+} are discussed in view of the measured KER spectra and the calculated potential energy curves of N_2O^{2+} .

2. Experimental approach

The experimental work was carried out in the laser lab of the (IKF) at the Frankfurt University, using the COLTRIMS setup presented in Fig. 1. This experimental setup has been discussed in detail in our previous work [25]. Briefly, 35 fs linearly polarized laser pulses (x -axis) with a central wavelength of 790 nm generated at a repetition rate of 8 kHz were used to ionize a molecular beam of N_2O molecules generated from a collimated supersonic gas jet (y -axis). The laser peak intensity is about 4.38×10^{14} W/cm² (with an error of about 10%). The electric field is polarized in the direction of the z -axis, which coincides with the time-of-flight (TOF) direction of the ion spectrometer. The ions and electrons emitted from the explosion of ionized N_2O molecule were directed by a combination of parallel electric and magnetic fields (14.5 V/cm and 8 G, respectively) onto two position-sensitive detectors with delay-line readout and detected in coincidence. All possible singly charged ions resulting from the dissociation of N_2O , namely N^+ , O^+ , N_2^+ , and NO^+ , were detected in our experiment.

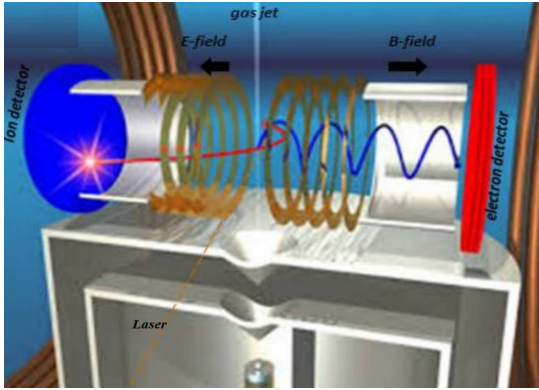


Fig. 1. Schematic diagram of the COLTRIMS experimental setup.

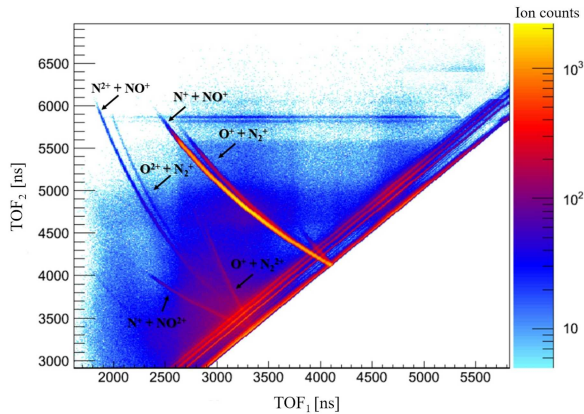
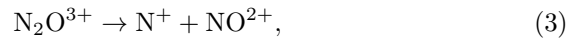


Fig. 2. TOF correlation map of ionic fragments, resulting from the dissociative ionization of N_2O induced by 35 fs linearly polarized laser pulses.

The three-dimensional momentum vectors of these ions are reconstructed from their measured times-of-flight and impact positions. Furthermore, we were able to determine the molecular axis from the measured momenta of the coincident ions. The axial recoil approximation [26] is successful in the breakup processes of the type considered here, in which the molecular dissociation process that follows molecular ionization is much faster than molecular rotation. Therefore we can neglect the geometric rotation effect of the molecule during the ionization and study the orientation-dependent ionization of the N_2O molecule without preorientation of the molecule. Thus the influence of the laser field on the N_2O can be seen in the alignment change of the molecular axis with respect to the direction of laser polarization.

3. Results and discussion

The TOF correlation map (PIPICO spectrum) of N_2O ionic fragments is shown in Fig. 2. The sharp lines seen in the PIPICO (PhotoIon-PhotoIon COincidence) spectrum are a consequence of the momentum conservation during the dissociation of the molecular ion. Thus, a number of fragmentation channels can be clearly identified. We first filtered the coincident events from the non-coincident ions by applying the momentum conservation principle. By selecting a narrow gate in the PIPICO spectrum for each fragmentation channel, the coincident events of each fragmentation channel have been distinguished from non-coincident events with very low uncertainty. Six coincidence channels of the dissociation of N_2O^{r+} ($r = 2, 3$) were identified as follows



The relative contributions of different double- and triple-ion coincidence channels were deduced from the coincident events in these channels. They are presented in Fig. 3. The results show that the $N^+ + NO^+$ fragmentation channel is the most dominant channel. Based on the abundance of different channels presented in Fig. 3, it is clear that the $O^+ + N_2^+$ fragmentation channel is the second most probable fragmentation channel. These experimental results presented in Fig. 3 are consistent with the limited available experimental and theoretical data [8, 9, 12, 13, 17, 23, 24]. In addition, the ratio of N_2O^{2+} breakup to $N^+ + NO^+$ and $O^+ + N_2^+$ was calculated and found to be about (3.3:1) for the present work. It is, to some extent, in agreement with the previous experimental and theoretical results [12, 13, 23]. This ratio is larger than the ratio

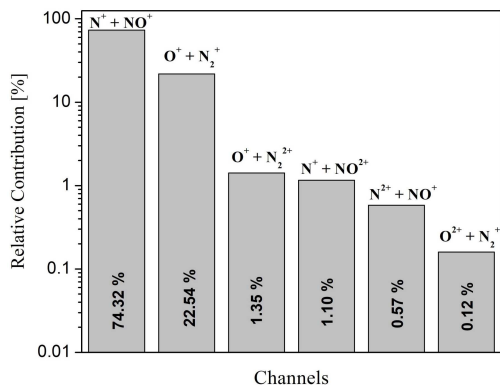


Fig. 3. Relative contribution of the six reaction channels observed in the dissociative ionization of nitrous oxide (N_2O) molecules induced by 35 fs linearly polarized laser pulses.

obtained for the ion experiment, which is about (1.4:1) [17], and for the electron experiment, which is about (3:1) [9]. The difference in the ratios could be due to the different dissociation mechanisms, leading to the formation of N_2O^{2+} excited-state populations. While they are the electron-capture processes in the ion-molecule collision, they are the pure ionizations in electron or photon collisions.

We also computed the contribution of singly, doubly, and triply ionized N_2O to a particular fragment ion yield. We found that about 81.90% of single ionization, about 17.36% of double ionization, about 0.57% of triple ionization, and < 0.20% of other ionization of the parent N_2O molecule contribute to the total fragment ion yield. This result suggests that the multiple ionization of N_2O makes a considerable contribution of about 18% to the total fragment ion yield in the present fragmentation process.

Using the time-of-flight and the detector hit position for each ion, the three-dimensional momentum of each ion can be reconstructed, and the total kinetic energy release (KER) spectrum for each ion and then for each channel can be extracted. In the present work, we focus on the dynamics of the completely measured two-body breakup channels, $N^+ + NO^+$ and $O^+ + N_2^+$, in which breakage of one N–N bond and one O–N bond occurred during fragmentation. The dynamics of the three-body breakup of N_2O will be targeted in a follow-up experiment. The specific KER distributions for the $N^+ + NO^+$ channel and their ions are shown in Fig. 4. Figure 4a shows the energy of the N^+ ion resulting from the fragmentation channel $N_2O^{2+} \rightarrow N^+ + NO^+$. The KER spectrum has been fitted using two Gaussian-type peaks. A major peak can be observed at $E = 4.55$ eV. Another peak, which is a shoulder or broad peak, can also be observed around $E = 6.62$ eV. The energy of the second fragment NO^+ ion resulting from $N_2O^{2+} \rightarrow N^+ + NO^+$ fragmentation channel is presented in Fig. 4b. A single peak can

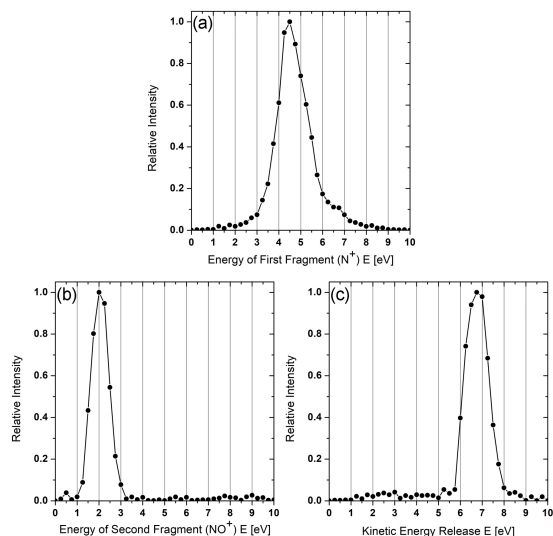


Fig. 4. KER distributions for (a) the first fragment N^+ ion, (b) the second fragment NO^+ ion and (c) the $N^+ - NO^+$ channel.

be seen at $E = 2.04$ eV. The KER distribution for the $N^+ + NO^+$ channel is shown in Fig. 4c. A single peak is shown at $E = 6.78$ eV. Based on the potential energy curves (PECs) of N_2O^{2+} calculated by Taylor et al. [14], we find that this peak can be explained by dissociation via the $X^3\Sigma^-$ and $1^3\Pi$ states of the N_2O dication. Accordingly, the single KER peak centered at $E = 6.78$ eV can be attributed to the significant contribution of the N_2O^{2+} ($X^3\Sigma^-$) dissociation pathway, in which the ground state $X^3\Sigma^-$ dissociates to $N^+(^3P) + NO^+(^1\Sigma^+)$ whose energy limit is $E = 28.8$ eV [27]. However, the $1^3\Pi$ state of N_2O^{2+} is also contributing to this single peak centered at $E = 6.78$ eV, as reported by Taylor et al. [14]. The explanation for this, is that N_2O^{2+} in the $1^3\Pi$ state may decay along the N–N stretching direction through fluorescent transitions into the $X^3\Sigma^-$ state and then dissociate to $N^+(^3P) + NO^+(^1\Sigma^+)$, resulting in the same KER [14, 21]. This major peak centered at $E = 6.78$ eV is in good agreement with the previous measurements [8, 17, 21, 28, 29].

The KER distributions for the $O^+ + N_2^+$ channel and the resulting ions are shown in Fig. 5. Each spectrum from the KER spectra has been fitted using two Gaussian-type peaks. Figure 5a shows the energy of the O^+ ion resulting from $N_2O^{2+} \rightarrow O^+ + N_2^+$ fragmentation channel. A major peak can be observed at $E = 3.72$ eV, and a shoulder or broad peak can be observed around $E = 6.08$ eV. The energy of the second fragment N_2^+ ion resulting from $N_2O^{2+} \rightarrow O^+ + N_2^+$ fragmentation channel is presented in Fig. 5b. A major peak can be seen at $E = 2.51$ eV. A broad peak can also be observed around $E = 4.36$ eV. The KER distribution for the $O^+ + N_2^+$ channel is shown in Fig. 5c. While a major peak can be observed at $E = 5.76$ eV,

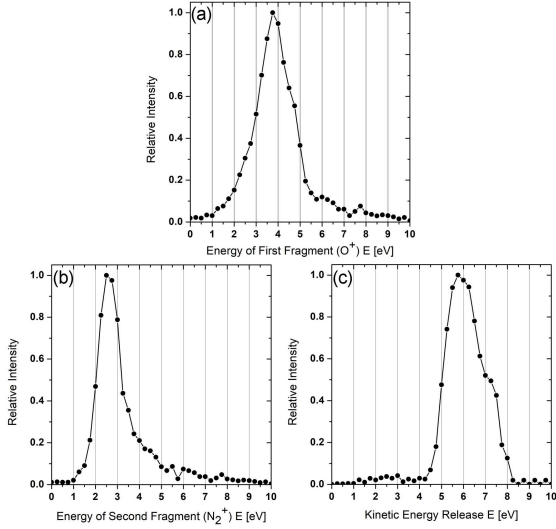


Fig. 5. KER distributions for (a) the first fragment O^+ ion, (b) the second fragment N_2^+ ion and (c) the $O^+ - N_2^+$ channel.

a broad peak can be observed around $E = 7.0$ eV. These observations on KER spectra are in good agreement with the previous measurements ($E = 5.8$ and $E = 7.2$ eV) [21]. We can again explain characteristics of these peaks in terms of the potential energy curves (PECs) of N_2O^{2+} [14]. The major peak centered at $E = 5.76$ eV can be interpreted as a result of the decay of the N_2O^{2+} ($X^3\Sigma^-$) into $O^+(^4S) + N_2^+(^2\Sigma_g^+)$ whose energy limit is $E = 30.9$ eV. The broad peak around $E = 7.0$ eV can be due to the decay of the N_2O^{2+} ($1^3\Pi$) into $O^+(^4S) + N_2^+(^2\Pi_u)$ whose energy limit is $E = 32.4$ eV.

The angular distributions of the fragment ions N^+ and NO^+ resulting from the denitrogenation of the N_2O dication ($N_2O^{2+} \rightarrow NO^+ + N^+$) and the fragment ions O^+ and N_2^+ resulting from the deoxygenation of the N_2O dication ($N_2O^{2+} \rightarrow O^+ + N_2^+$) were also studied. These angular distributions are presented in Figs. 6 and 7. Note that the laser polarization vector is oriented horizontally and indicated by the black arrows. Figure 6a shows the angular distribution of N^+ ion resulting from the denitrogenation of the N_2O dication. This distribution shows a markedly anisotropic behavior. It is peaked at $\theta = 0$ and $\theta = \pm 180^\circ$, i.e., in the horizontal emission direction and at $\theta = \pm 90^\circ$, i.e., in the vertical emission direction. These peaks can be clearly seen in the polar view of the N^+ angular distribution presented in Fig. 6b. Similar observations have been reported in several previous studies [29–31]. These anisotropic behaviors in the N^+ angular distributions can be attributed to the combined effect of two main conditions: (i) the fragmentation of the two non-equivalent Nitrogen atoms in the N_2O molecule, (ii) the different orientations of the N_2O molecule relative to the laser polarization

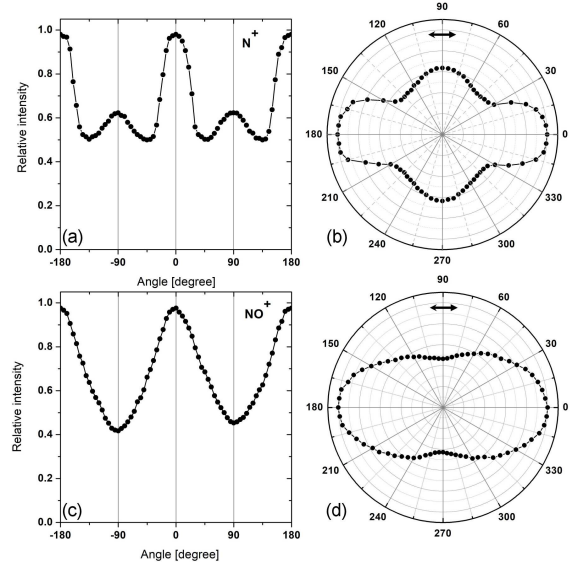


Fig. 6. Angular distribution of the first fragment N^+ ion (a), polar view angular distribution of the first fragment N^+ ion (b), angular distribution of the second fragment NO^+ ion (c), and polar view angular distribution of the second fragment NO^+ ion (d). The black arrows in (b, d) indicate the polarization direction of the laser field.

vector during the fragmentation. In other words, when the N_2O molecular axis and polarization vector are collinear, then the transient molecule N_2O^{2+} will achieve a higher ionization stage than when the molecule and polarization are orthogonal. Thus, for the horizontal polarization, the peripheral ions, resulting from the fragmentation of the N_2O molecule along the field, are directed along TOF-axis, and for vertical polarization, it is the central atom that is so directed. Figure 6c displays the angular distribution of NO^+ ion resulting from the denitrogenation of the N_2O dication. It is remarkable that the angular distribution of NO^+ behaves in a different way than the angular distribution of N^+ . The angular distribution of NO^+ ion is also anisotropic. Peaks at $\theta = 0$ and $\theta = \pm 180^\circ$ (horizontal emission direction) are clearly observed in the NO^+ angular distribution. For the vertical emission direction ($\theta = \pm 90^\circ$), a reduction in the ion yields is seen in the angular distribution of NO^+ ion, which differs from what is observed for the N^+ angular distribution. Such different behavior can be clearly seen in the polar view of the NO^+ angular distribution presented in Fig. 6d.

Figure 7 shows the angular distributions of the fragment ions O^+ and N_2^+ resulting from the deoxygenation of the N_2O dication ($N_2O^{2+} \rightarrow O^+ + N_2^+$). The angular distribution of O^+ ion is presented in Fig. 7a. The angular distribution is also anisotropic. The distribution is peaked at $\theta = 0$ and $\theta = \pm 180^\circ$, i.e., in the horizontal emission direction. In addition, a large reduction in the ion

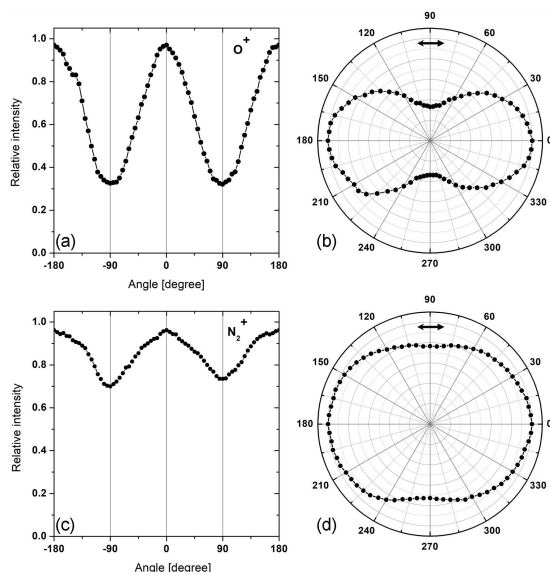


Fig. 7. Angular distribution of the first fragment O⁺ ion (a), polar view angular distribution of the first fragment O⁺ ion (b), angular distribution of the second fragment N₂⁺ ion (c), and polar view angular distribution of the second fragment N₂⁺ ion (d). The black arrows in (b, d) indicate the polarization direction of the laser field.

yield for the vertical emission direction ($\theta = \pm 90^\circ$) can be clearly seen in the angular distribution. This is shown clearly in polar view of the O⁺ angular distribution presented in Fig. 7b. This behavior is in contrast to what is observed in the angular distribution of N₂⁺ ion shown in Fig. 7c and d. A moderate reduction in the ion yield for the vertical emission direction ($\theta = \pm 90^\circ$) can be observed in the angular distribution of N₂⁺ ion. However, similar peaks at $\theta = 0$ and $\theta = \pm 180^\circ$, i.e., in the horizontal emission direction that are observed in the angular distribution of O⁺ ion are also seen in the angular distribution of N₂⁺ ion.

4. Conclusions

We investigated the dissociative ionization of nitrous oxide molecules induced by linearly polarized intense femtosecond laser pulses. The coincident measured times of flight of the first and the second fragment ions are used to identify the different dissociation channels. The coincident TOF spectrum is also used to deduce the relative contributions of different double and triple dissociative ionization channels to the total fragment ion yield. The results show that a significant contribution to the total fragment ion yield arises from the double dissociative ionization channels, i.e., denitrogenation ($\text{N}_2\text{O}^{2+} \rightarrow \text{N}^+ + \text{NO}^+$) and deoxygenation ($\text{N}_2\text{O}^{2+} \rightarrow \text{O}^+ + \text{N}_2^+$). Furthermore, a considerable contribution of the triple dissociative ionization channels to the total fragment ion yield

is also observed. The kinetic energy release distributions measured for different dissociation channels are used to determine different pathways leading to these dissociation channels involving various bound and repulsive states of the N₂O dication. The N⁺ + NO⁺ and O⁺ + N₂⁺ fragmentation channels are explained by the decay via the X ³Σ⁻ and 1 ³Π states of N₂O²⁺ as the major peaks in the KER spectra suggested. The angular distributions of the fragment ions N⁺, NO⁺, O⁺, and N₂⁺ resulting from the N⁺ + NO⁺ and O⁺ + N₂⁺ fragmentation channels were also measured. The distributions show a markedly anisotropic behavior. These anisotropic behaviors in the angular distributions can be attributed to the different orientations of the N₂O molecule relative to the laser polarization during the fragmentation process.

Acknowledgments

We gratefully acknowledge support from the Deutsche Forschungsgemeinschaft (DFG), J.W. Goethe (Frankfurt) University and the Hashemite University. We are also indebted to Prof. Reinhard Dörner and Prof. Horst Schmidt-Böcking for their helpful support.

References

- [1] *Imaging in Molecular Dynamics—Technology and applications*, edited by B. Whitaker, Cambridge University Press, New York, 2003.
- [2] R. Dörner, V. Mergel, O. Jagutzki, L. Spielberger, J. Ullrich, R. Moshhammer, H. Schmidt-Böcking, *Phys. Rep.* **330**, 95 (2000).
- [3] J. Ullrich, R. Moshhammer, A. Dorn, R. Dörner, L.P.H. Schmidt H. Schmidt-Böcking, *Rep. Prog. Phys.* **66**, 1463 (2003).
- [4] A. Hishikawa, A. Iwamae, K. Yamanouchi, *Phys. Rev. Lett.* **83**, 1127 (1999).
- [5] N. Neumann, D. Hant, L.P.H. Schmidt, J. Titze, T. Jahnke, A. Czasch, M. S. Schöffler, K. Kreidi, O. Jagutzki, H. Schmidt-Böcking, and R. Dörner, *Phys. Rev. Lett.* **104**, 103201 (2010).
- [6] I. Bocharova, R. Karimi, E.F. Penka, J.-P. Brichta, P. Lassonde, X. Fu, J.-C. Kieffer, A.D. Bandrauk, I. Litvinyuk, J. Sanderson, F. Légaré, *Phys. Rev. Lett.* **107**, 063201 (2011).
- [7] A.R. Ravishankara, J.S. Daniel, R.W. Portmann, *Science* **326**, 123 (2009).
- [8] A. Khan, D. Misra, *J. Phys. B: At. Mol. Opt. Phys.* **49**, 055201 (2016).
- [9] P. Bhatt, R. Singh, N. Yadav, R. Shanker, *Phys. Rev. A* **86**, 052708 (2012).

- [10] N.A. Love, S.D. Price, *Phys. Chem. Chem. Phys.* **6**, 4558 (2004).
- [11] J.H.D. Eland, V.J. Murphy, *Rapid Commun. Mass Spectrom.* **5**, 221 (1991).
- [12] M. Alagia, P. Candori, S. Falcinelli, M. Lavollée, F. Pirani, R. Richter, S. Strangesb, F. Vecchiocattivi, *Chem. Phys. Lett.* **432**, 398 (2006).
- [13] S.D. Price, J.H.D. Eland, P.G. Fournier, J. Fournier, P. Millie, *J. Chem. Phys.* **88**, 1511 (1988).
- [14] S. Taylor, J.H.D. Eland, M. Hochlaf, *J. Chem. Phys.* **124**, 204319 (2006).
- [15] D.M. Curtis, J.H.D. Eland, *Int. J. Mass Spectrom. Ion Processes* **63**, 241 (1985).
- [16] X. Zhou, P. Ranitovic, C.W. Hogle, J. Eland, H. Kapteyn, M. Murnane, *Nat. Phys.* **8**, 232 (2012).
- [17] B. Siegmann, U. Werner, H.O. Lutz, R. Manny, *GSI Scientific Report* **2002**, 100 (2003).
- [18] D. Wang, G. Guo, G. Min, X. Zhang, *Phys. Rev. A* **95**, 012705 (2017).
- [19] U. Werner, B. Siegmann, R. Mann, in: *GSI Scientific Report 2006*, GSI, Darmstadt 2007, p. 113.
- [20] A. Khan, L. C. Tribedi, D. Misra, *Phys. Rev. A* **96**, 012703 (2017).
- [21] M. Kübel, A.S. Alnaser, B. Bergues et al., *New J. Phys.* **16**, 065017 (2014).
- [22] A. Hishikawa, A. Iwamae, K. Hoshina, M. Kono, K. Yamanouchi, *Res. Chem. Intermed.* **24**, 765 (1998).
- [23] M. Ueyama, H. Hasegawa, A. Hishikawa, K. Yamanouchi, *J. Chem. Phys.* **123**, 154305 (2005).
- [24] N. Levasseur, P. Millié, *J. Chem. Phys.* **92**, 2974 (1990).
- [25] F. Afaneh, H. Schmidt-Böcking, *Int. J. Mod. Phys. B* **31(29)**, 1750215 (2017).
- [26] R.N. Zare, *Mol. Photochem.* **4**, 1 (1972).
- [27] R. Murphy, W. Eberhardt, *J. Chem. Phys.* **89**, 4054 (1988).
- [28] Lei Chen, Xu Shan, Xi Zhao et al., *Phys. Rev. A* **99**, 012710 (2019).
- [29] P. Graham, X. Fang, K.W.D. Ledingham, R.P. Singhal, T. Mccanny, D.J. Smith, C. Kosmidis, P. Tzallas, A.J. Langley, P.F. Taday, *Laser Part. Beams* **18**, 417 (2000).
- [30] P. Graham, K.W.D. Ledingham, R.P. Singhal et al., *J. Phys. B* **32**, 5557 (1999).
- [31] P. Graham, K.W.D. Ledingham, R.P. Singhal, T. Mccanny, S.M. Hankin, X. Fang, P. Tzallas, C. Kosmidis, P.F. Taday, A.J. Langley, *J. Phys. B* **33**, 3779 (2000).